11. L. A. Savintseva, V. L. Chastyi, and A. V. Sharkov, "Analysis of the internal heat source intensity in systems containing highly intensive radiation sources," Izv. Vyssh. Uchebn. Zaved., Priborostr., 21, No. 3, 102-106 (1978).
12. G. N. Dul'nev and É. M. Semyashkin, Heat Exchange in Radio Electronic Apparatus [in Russian], Énergiya, Leningrad (1968).
13. H. Wong, Fundamental Formulas and Data on Heat Transfer for Engineers [Russian translation], Atomizdat, Moscow (1979).
14. S. S. Kutateladze and V. M. Borishanskii, A Concise Encyclopedia of Heat Transfer, Pergamon (1966).
15. G. N. Dul'nev and A. Yu. Potyagilo, "Nonstationary thermal mode of a system of bodies with internal energy sources," Tr. Leningr. Inst. Tochn. Mekh. Opt., No. 86, Analysis of Temperature Fields of Solids and Systems, 13-28 (1976).
16. B. I. Stepanov (ed.), Methods of Analyzing Lasers [in Russian], Vol. 2, Nauka i Tekhnika, Minsk (1968).

ANALYSIS OF THE THREE-DIMENSIONAL SELECTIVE RADIATION FIELD IN A COMBUSTION CHAMBER USING MATHEMATICAL MODELING

Yu. A. Zhuravlev, A. G. Blokh, and I. V. Spichak

UDC 536.3

Using the zonal method, the spectral structure of radiation fluxes over the height of furnace baffles in the BKZ-320-140 PT steam generator, appearing with the combustion of lignite in the combustion chamber, is investigated.

Improving furnaces that are presently in operation and designing new efficient furnaces, as well as optimizing their thermal operation, impose increasingly stringent requirements on the accuracy and detail of heat-exchange calculations. Of special significance in this connection is the determination and analysis of the temperature distribution and the heat-flux distribution in combustion chambers with the help of zonal methods taking into account the actual radiation properties of the media and bodies participating in heat exchange.

In the present work, using the zonal method, we analyze heat transfer in the combustion chamber of the BKZ-320-140 PT steam generator burning lignites from the Kansk–Achinski coal field. In so doing, we investigate for the first time the spectral structure of the radiation field under the conditions of three-dimensional multizone systems with a complex configuration, filled with a thermally and optically inhomogeneous medium having real radiation characteristics, using a computational method applicable to furnaces. The spectral structure is important for determining the effect of the radiation properties of the furnace medium and of the heat-absorbing surfaces on indicators of local and total heat transfer in the combustion chamber.

In the calculations, we investigated the multizone mathematical model of heat transfer [1]. The geometric volume of the combustion chamber and the vertical surfaces of the baffles were represented as seven computational regions, each of which consisted of two volume regions (near-wall region and the core of the flow) and three surface (lateral, frontal, and rear baffles) regions. We calculated the heat exchange for coal consumption of 51,606 tons/h. The mathematical model and the scheme for separating the combustion chamber into zones are presented in [1].

Taking into account the nonuniformity of the vertical thickness distribution of ash deposits on the furnace baffles in the combustion chamber is important for studying the local values of temperature and radiation fluxes. Starting from the assumption that the thickness of the deposits varies linearly with the height of the cooling chamber, the magnitudes of the thermal resistance R_i in the computational region i were found from the relation

M. I. Kalinin Institute of Nonferrous Metals, Krasnoyarsk. Scientific Industrial Union of the I. I. Polzunov Central Boiler and Turbine Institute (NPO TsKTI). Translated from Inzhenerno-Fizicheskii Zhurnal, Vol. 41, No. 1, pp. 119-128, July, 1981. Original article submitted April 16, 1980.

0022-0841/81/4101-0762$07.50

TABLE 1. Emissivities, Averaged over the Width of the Spectral Intervals, of the Slag Film $\varepsilon_{sl}^{\lambda}$, Ash Deposits $\varepsilon_{a}^{\lambda}$, and Flame $\varepsilon_{f}^{\lambda}$ (at different distances h along the height of the combustion chamber)

Spectral interval, μm		ε_f^λ			ε_{sl}^λ	ε_a^λ
λ_{init}	λ_{fin}	h=2,75m	h=12,7m	h=17,9 m		
0,875	1,125	0,28	0,19	0,15	0,92	0,30
1,125	1,375	0,40	0,27	0,20	0,98	0,34
1,375	1,625	0,56	0,35	0,26	0,96	0,38
1,625	1,875	0,76	0,67	0,51	0,94	0,43
1,875	2,125	0,48	0,42	0,34	0,92	0,47
2,125	2,375	0,69	0,64	0,53	0,88	0,55
2,375	2,625	0,90	0,89	0,87	0,85	0,62
2,625	2,875	0,999	0,999	0,999	0,83	0,68
2,875	3,125	0,69	0,64	0,53	0,80	0,72
3,125	3,375	0,60	0,48	0,38	0,77	0,77
3,375	3,625	0,53	0,41	0,36	0,74	0,80
3,625	3,875	0,57	0,43	0,37	0,71	0,84
3,875	4,125	0,80	0,70	0,50	0,69	0,86
4,125	4,375	0,999	0,999	0,999	0,67	0,88
4,375	4,625	0,81	0,77	0,74	0,65	0,89
4,625	4,875	0,74	0,67	0,65	0,63	0,90
4,875	5,325	0,68	0,63	0,61	0,60	0,90
5,325	6,00	0,64	0,59	0,59	0,60	0,87
6,00	7,00	0,62	0,58	0,58	0,60	0,82
7,00	8,00	0,63	0,57	0,57	0,60	0,81
8,00	9,00	0,60	0,52	0,51	0,60	0,81
9,00	10,00	0,57	0,50	0,48	0,60	0,80

Note. The values of $\varepsilon_{sl}^{\lambda}$ for $\lambda > 4$ μm and $\varepsilon_{a}^{\lambda}$ for $\lambda > 5$ μm were obtained by extrapolation.

$$R_i = R_{av} \frac{[(H - h_i)(n' - n'') + H] \sum_i F_{r,i}}{\sum_i F_{r,i} [(H - h_i)(n' - n'') + H]}. \quad (1)$$

In the calculations presented in what follows, taking into account the practice and recommendations of the standard methods [2], we assume $R_{av} = 0.0034$ m²·°C/W, n' = 1.1, and n" = 0.9. The model also took into account the nonuniformity in the vertical infiltration distribution in the combustion chamber (with overall air infiltration equal to 0.05 [2]).

The spectral emissivities of the flame $\varepsilon_{f}^{\lambda}$ at different points along the vertical in the combustion chamber in the wavelength range $\lambda < 5$ μm were determined from the values of the incident spectral radiation fluxes, obtained experimentally with the help of a portable spectrograph on the Irkutsk TÉTs-6 boiler being studied with the combustion of Beryozov coal. In the spectral range from 5 to 10 μm, the emissivity of the dispersed phase was obtained by extrapolating based on the relations in [3], while the emissivities of triatomic gases were calculated from data in [4, 5] based on the statistical model of the absorption band. The spectral emissivities of the flame that were used, as well as the liquid slag film and the ash deposits [6], are presented in Table 1.

In order to calculate the radiative heat exchange in the combustion chamber, we separated the spectral range of the radiation (from 0.875 to 10 μm) that was taken into account into z = 22 intervals $\Delta\lambda_k$. The use of a large number of spectral intervals results from the complex nature of the change in the radiation characteristics of the coal-dust flame, ash deposits, and slag, possibility of performing a detailed analysis of the effect of the selectivity of the radiation on the heat-exchange pattern in the combustion chamber, as well as the necessity for having a quite accurate scale for evaluating engineering solutions, when the spectrum is separated into a smaller number of intervals.

The values of the temperatures and the radiation fluxes were determined from the solution of a system of equations for heat transfer and the thermal balance of the zones, taking into account, in addition to radiative heat transfer, convective and heat transfer through the layer of ash deposits or the liquid slag film, heat transfer to the moving medium, and heat liberation due to fuel combustion:

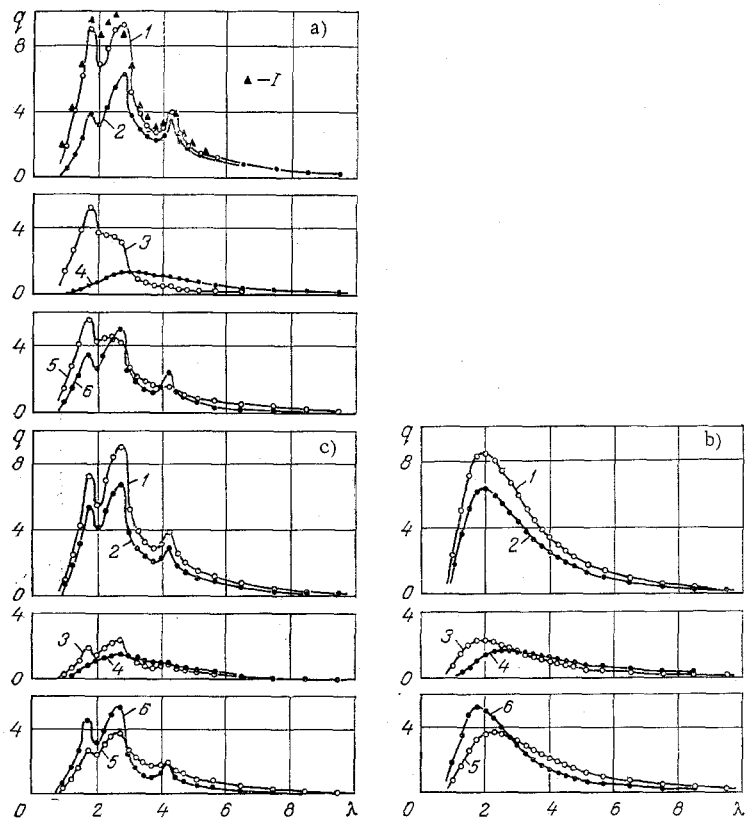

Fig. 1. Densities of incident (1), absorption (2), reflected (3), characteristic (4), effective (5), and resulting (6) radiation fluxes q ($W/cm^2 \cdot \mu m$) averaged over the area of the zone with the lateral buffles in the cooling chamber (average vertical distance in the combustion chamber is 13.4 m) as a function of wavelength λ (μm); a) for variant 1 (I indicates the experimental values); b) for variant 2; c) for variant 3.

$$4\sigma_0 \sum_{i=1}^{m} V_i T_i^4 \sum_{k}^{z} \alpha_i^k (f_{ij}^k - \delta_{ij}) \mu_i^k + \sigma_0 \sum_{i=m+1}^{m+n} F_i T_i^4 \sum_{k}^{z} \varepsilon_i^k (f_{ij}^k - \delta_{ij}) \mu_i^k + \sum_{i=1}^{l} g_{ij} T_i - g_{jj} T_j + Q_j = 0, \tag{2}$$

$$\delta_{ij} = \begin{cases} 1, & i = j; \\ 0, & i \neq j, \end{cases} \quad j = 1, 2, \ldots, m+n.$$

The sequence of calculations of the coefficients of convective heat transfer g_{ij} and the free terms Q_j in Eqs. (2), applicable to combustion chambers, is presented in [1].

The values of the longitudinal resulting radiation fluxes through the transverse cross section of the combustion chamber in the spectral range of interval k was determined from the relation

$$Q_{\text{long}}^k = \sum_{j^*} \sum_{i^*} (a_{i^* j^*}^k T_{i^*}^4 - a_{j^* i^*}^k T_{j^*}^4). \tag{3}$$

In (3), the index i* labels the zones situated on one side of the combustion chamber cross section being examined; j* labels the zones on the other side; $a^k{}_{i^*, j^*}$ are the spectral radiative transfer coefficients, W/K^4 [1].

The zone averaged values of the radiation flux densities for surface zones in the spectral range of the k-th interval are found from the following relations:

for incident radiation

$$q_{\text{inc}, i}^k = \frac{\sigma_0}{\varepsilon_j^k F_j} \left(4 \sum_{i=1}^{m} \alpha_i^k V_i f_{ij}^k \mu_i^k T_i^4 + \sum_{i=m+1}^{m+n} \varepsilon_i^k F_i f_{ij}^k \mu_i^k T_i^4 \right), \tag{4}$$

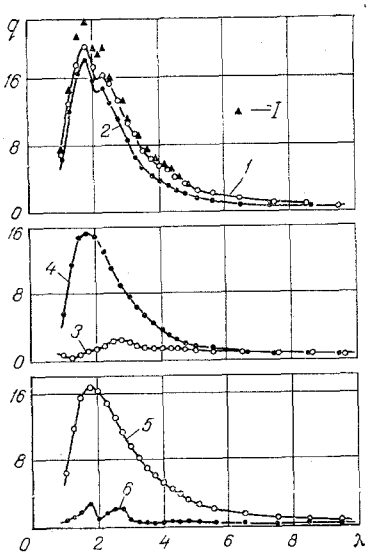

Fig. 2. Radiation flux densities q averaged over the surface area of the lateral studded baffle in the lower part of the combustion chamber (average distance along the height of the combustion chamber, 1.5 m) as a function of wavelength λ for variant 1. The labels are the same as in Fig. 1.

for characteristic radiation

$$q^k_{\mathrm{ch},j} = \sigma_0 \varepsilon^k_j \mu^k_j T^4_j . \tag{5}$$

The flux densities of the absorbed, reflected, effective, and resulting radiation were determined from equations coupling the different forms of radiation fluxes based on the spectral dependences of the emissivities of the surfaces studied.

Figures 1 and 2 show the computed spectral dependences for various types of radiation flux densities for parts of the lateral baffles, located at a height of 13.4 m (center of the cooling chamber, Figs. 1a, b, and c) and 1.5 m (lower part of the combustion chamber, Fig. 2) from the bottom of the combustion chamber. Four variants were examined: 1) a selective medium and a selective surface (Figs. 1a and 2); 2) gray medium, gray surface (Fig. 1b); 3) selective medium, gray surface (Fig. 1c); 4) gray medium, selective surface.

As can be seen from the data presented, the spectral composition of the incident radiation is to a large extent determined by the radiation characteristics of the medium in the combustion chamber. Thus, for a selective medium, sharp peaks are observed in the radiation flux densities for the center of the cooling chamber in the region $\lambda = 1.75$, 2.75, and 4.25 μm (Figs. 1a and c), and in the region $\lambda = 1.75$ μm for the combustion chamber (Fig. 2). The disappearance of the peak at $\lambda = 4.25$ μm and intensification of the peak at $\lambda = 1.75$ μm passing from the cooling to the combustion chamber is due to the high temperature and emissivity of the flame at $\lambda = 1.75$ μm for the combustion chamber. For a gray medium, both in the cooling (Fig. 1b) and combustion chambers, there is a smooth radiation spectrum.

However, for the same medium in the cooling chamber, the nature of the incident radiation is not the same. Thus, for a selective medium, for selective surfaces (Fig. 1a), a more clearly manifested, in comparison to gray surfaces (Fig. 1c), incident radiation is observed in the short wavelength part of the spectrum, which stems from the high reflectivity (0.5-0.7) of the ash deposits in the wavelength range up to 2 μm. Similarly, in the case of a gray medium, the selectivity of the radiation from the walls increases $q^{\lambda}_{\mathrm{inc}}$ in the wavelength range up to 3 μm. In the combustion chamber, the nature of the radiation from the walls has practically no effect on the spectral structure of the radiation fluxes.

Comparison of the computed and experimentally measured values of $q^{\lambda}_{\mathrm{inc}}$ (see Figs. 1a and 2) indicates their quite good agreement, taking into account the multistage nature and the cumbersomeness of the calculations, the use of data in the literature on the emissivities of slag and ash deposit surfaces in the form of graphs and averaging them over spectral intervals, as well as the necessity to extrapolate them into the range 5-10 μm. It is also necessary to keep in mind that the experimental data correspond to local values of the incident flux, while the computed data correspond to values averaged over the area of the lateral baffle zone being examined. The magnitude of the disagreement between the computed and experimental values could also be affected (in accordance with Planck's law) by the error in the experimental determination of the temperature of the medium in the furnace. It should be noted that in the spectrum of the incident radiation, obtained experimentally, a local minimum is observed in the range $\lambda = 2.00$-2.25 μm. This effect is not brought out in the calculations due to the small subdivision of the range being studied.

TABLE 2. Values of Spectral and Integral Thermal Efficiency Coefficients $\psi = q_{res}/q_{inc}$ for the Lateral Baffles at Different Vertical Distances in the Combustion Chamber

λ_{av} μm	Vertical distance in combustion chamber, m						
	comb. chamber	cooling chamber					
	1,5	4,44	7,36	10,33	13,39	16,95	21,43
1,00	0,053	0,011	0,266	0,281	0,290	0,294	0,300
1,25	0,078	0,036	0,284	0,305	0,318	0,329	0,337
1,50	0,104	0,066	0,302	0,327	0,342	0,359	0,371
1,75	0,143	0,113	0,338	0,365	0,381	0,398	0,412
2,00	0,056	0,022	0,317	0,354	0,377	0,405	0,430
2,25	0,095	0,068	0,374	0,382	0,437	0,465	0,491
2,50	0,131	0,100	0,433	0,475	0,496	0,526	0,549
2,75	0,158	0,108	0,487	0,523	0,545	0,580	0,600
3,00	0,070	0,046	0,407	0,459	0,484	0,515	0,549
3,25	0,047	0,039	0,376	0,409	0,477	0,479	0,520
3,50	0,031	0,023	0,349	0,398	0,419	0,454	0,499
3,75	0,031	0,021	0,353	0,400	0,418	0,449	0,494
4,00	0,068	0,048	0,429	0,483	0,495	0,505	0,524
4,25	0,100	0,070	0,540	0,587	0,609	0,647	0,669
4,50	0,064	0,046	0,434	0,490	0,508	0,536	0,555
4,75	0,052	0,033	0,401	0,455	0,469	0,497	0,517
5,125	0,040	0,021	0,372	0,426	0,440	0,464	0,483
5,688	0,034	0,017	0,338	0,385	0,397	0,421	0,435
6,50	0,031	0,016	0,308	0,349	0,358	0,373	0,383
7,50	0,031	0,015	0,292	0,329	0,335	0,345	0,348
8,50	0,026	0,010	0,269	0,301	0,301	0,303	0,305
9,50	0,023	0,009	0,258	0,289	0,288	0,287	0,282
Integral values	0,067	0,042	0,360	0,399	0,432	0,438	0,457

Analysis of the transformation of the spectral composition of radiation in the presence of interaction with contaminated baffle surfaces is of practical interest for optical and radiation pyrometry, as well as for clarifying the mechanism for the effect of the selectivity of the radiation on the heat-transfer picture.

The spectral composition of the reflected and absorbed radiation is determined by the composition of the incident radiation and the spectral radiation characteristics of the heat absorbing surfaces. Comparing the incident, reflected, and absorbed radiation at the center of the cooling chamber, it is evident that the sharp increase with increasing wavelength in the near-infrared range of the spectral emissivity of ash deposits leads to significant transformation of the spectral composition of the incident radiation. At the same time, peaks in the short wavelength (up to 2 μm) part of the spectrum are sharply increased and are smoothed out in the long wavelength part in the radiation reflected by the baffles in the cooling chamber.

The sharp peak in the reflected radiation at $\lambda = 1.75$ μm for the selective model (Fig. 1a), which is explained by the presence of one of the absorption bands of H_2O and the high reflectivity (0.57) of the ash deposits in this range of the spectrum, attracts attention. At the same time, we note the absence of a peak at a wavelength of 2.75 μm in the reflected radiation (curve 3 in Fig. 1a), in spite of the intense incident radiation (curve 1, Fig. 1a) in this region of the spectrum. The peak in the reflected radiation in the 4.3-μm region of the radiation band is also insignificant. This stems from the decrease in the reflectivity of ash deposits from 0.53 at $\lambda = 2.00$ μm to 0.32 at $\lambda = 2.75$ μm.

In spite of the higher values of the incident radiation flux ($q^{\lambda}_{inc} = 19.64$ W/cm$^2\cdot$μm), for the combustion chamber at $\lambda = 1.75$ μm lower values of the reflected radiation ($q^{\lambda}_{ref} = 1.18$ W/cm$^2\cdot$μm) are observed compared to the cooling chamber (see Figs 1a and 2), which stems from the higher emissivity of the slag compared to the ash deposits in this region of the spectrum. At the same time, since the reflectivity of the slag film increases with wavelength (see Table 1), for real surfaces the maximum in the reflected radiation is observed to shift toward the long wavelength part of the spectrum ($\lambda = 2.75$ μm) compared to gray surfaces ($\lambda = 1.75$ μm).

As can be seen from the data presented (see Figs. 1a and 2), the nature of the transformation of the incident radiation into absorbed radiation for the baffles in the cooling and combustion chambers is not the same. In the first case (Fig. 1a), the long wavelength radiation is relatively intensified, and at the same time, the peaks in the region of the absorption bands of gases at 2.7 and 4.3 μm are more sharply manifested. In the combustion chamber, on the other hand, transformation of the incident radiation into absorbed radiation is accompanied by an increase in the relative role of short wavelength radiation. At the same time, the local maximum at $\lambda = 1.75$ μm in the absorbed radiation in more clearly manifested than in the incident radiation (Fig. 2).

TABLE 3. Values of the Longitudinal Resulting Radiation Flux Densities (kW/m^2) in the Spectral Intervals through the Transverse Cross Section of the Furnace

λ_{av} μm	Vertical distance in furnace, m					
	3,00	5,88	8,83	11,83	14,95	18,95
1,00	3,32	9,92	4,71	4,12	4,08	2,32
1,25	5,56	17,11	8,67	8,15	8,45	4,93
1,50	6,12	19,99	11,06	11,25	12,04	7,24
1,75	5,4	14,98	9,79	12,145	14,96	9,64
2,00	5,62	19,30	8,93	9,44	11,28	7,67
2,25	4,20	13,83	7,29	9,13	11,64	8,14
2,50	3,09	7,51	3,76	7,13	9,74	7,70
2,75	3,45	0,41	2,55	3,82	6,17	6,07
3,00	2,50	9,04	4,23	5,23	6,901	5,11
3,25	2,42	9,06	4,19	4,47	5,30	3,96
3,50	2,14	8,05	3,58	3,63	4,101	3,161
3,75	2,111	6,92	3,06	3,05	3,48	2,72
4,00	1,12	4,16	1,98	2,760	3,66	2,70
4,25	0,962	0,01	0,55	1,02	1,93	2,00
4,50	0,73	2,66	1,12	1,57	2,18	1,80
4,75	0,68	2,61	1,10	1,36	1,75	1,51
5,125	1,07	3,72	1,53	1,87	2,44	2,14
5,6875	1,15	4,44	1,75	1,96	2,50	2,25
6,50	1,01	3,94	1,52	1,71	2,24	2,05
7,50	0,60	2,36	0,89	0,98	1,30	1,18
8,50	0,39	1,56	0,59	0,64	0,81	0,73
9,50	0,23	1,01	0,38	0,40	0,51	0,46
Integral values over the spectrum	53,88	162,57	83,23	95,79	117,46	85,46

A property of the characteristic radiation of ash deposits with real radiation characteristics (variant 1) compared to gray surfaces (variant 2) is the smaller magnitude of the radiation flux (expecially for $\lambda \lesssim 3$ μm) and a certain shift in its maximum toward longer wavelengths (Figs. 1a and b), which is explained by the lower temperature of the surfaces of the ash deposits in the zone being examined (for variant 1, t_a = 766°C and for variant 2 t_a = 814°C) and by increase in their emissivities with respect to wavelength (see Table 1). The relatively high values of the characteristic radiation in the short wavelength part of the spectrum in the lower part of the precombustion chamber (see Fig. 2) are explained by the high absorptivity of the slag and the high blackbody radiation density at the temperature of liquid slag removal.

The nature of the spectral distribution of the effective radiation, which appears as the sum of the reflected and characteristic radiation, for the center of the cooling chamber (Fig. 1a) in the range $\lambda < 3$ μm is determined primarily by the reflected radiation, while in the range $\lambda > 3$ μm, it is determined by the characteristic radiation of the ash deposits on the flues. In the lower part of the combustion chamber, the effective radiation is almost entirely (see Fig. 2) determined by the characteristic radiation.

The spectral structure of the resulting radiation flux, which is represented by the difference of the absorption and characteristic radiation, for the cooling chamber is close in nature and magnitude to the absorbed radiation, but the local minimum in the region λ = 3-4 μm comes through more sharply, which is explained by the considerable characteristic radiation of the surfaces with ash deposits in this region (Fig. 1a). For the combustion chamber, the magnitude and spectral composition for absorbed and resulting radiation are different (Fig. 2). Here, the spectral structure of the resulting flux is not the same for gray and selective media. In the case of a gray medium, there is a smoother radiation spectrum, while for the selective medium for λ = 1.75 and 2.75 μm sharp peaks are observed in the values of the heat flux (Fig. 2). The local maximum at λ = 1.75 μm is explained by the presence of a peak in the absorbed flux for this spectral region, while for λ = 2.75 μm it is explained by the nature of the change in the absorbed and characteristic radiation relative to one another in the adjoining parts of the spectrum (a greater decrease in the characteristic radiation in the region λ = 2.10-2.75 μm and a greater decrease in absorbed radiation in the region λ = 2.75-3.50 μm).

Calculations show that the density of incident radiation fluxes for the side baffles is greater than for the corresponding zones of the front baffle, situated at the same height from the bottom. Thus, the values of the radiation fluxes integrated over the spectrum for the combustion chamber with the transition from the side baffle to the front baffle decrease approximately by 15%, and for the center of the cooling chamber ($h \approx 13.4$ m) this decrease constitutes 4.9%. Such a decrease in the spectral radiation fluxes is to a large extent determined by the magnitude of the optical density of the medium in a particular part of the spectrum. At the same time, the decrease in the radiation fluxes in the spectral interval with a low value of the absorption coefficient (λ = 1.00 μm) constitutes 12% for the combustion chamber and 1% for the cooling chamber, and in the spectral

interval with an optically dense medium ($\lambda = 2.75\ \mu m$), the decrease for the combustion chamber equals 16% and 8% for the cooling chamber. The decrease in the radiation fluxes accompanying the transition from the lateral baffle to the front baffle is explained by the decrease in the effective path length of a ray with flame emission onto the baffle. It should be noted that in spite of the decrease in magnitude indicated above, the nature of the spectral distribution of the radiation fluxes for the front baffle is similar to that for the side baffle.

Analysis of the thermal efficiency coefficient distributions ψ over the height of the combustion chamber (Table 2), obtained for the conditions being examined, indicates the considerable change in ψ over the spectrum. In this case, the maximum values of ψ (0.49-0.67) occur for spectral intervals with flame emissivities close to unity. The smallest values of ψ (0.27-0.30) are observed for spectral intervals with low (0.15-0.28) flame emissivities. Some increase is evident in the spectral and integral thermal efficiency coefficients over the height of the cooling chamber, which is explained, apparently, by the distribution used for the thickness of the ash deposits over the height of the baffles. Considerably lower (0.04-0.07) integral values of ψ for the combustion chamber compared to the cooling chamber (0.40-0.50) are explained by the high temperature of the surface of the liquid film ($\approx$ 1370°C) on the lined baffles of the combustion chamber. The values of the thermal efficiency coefficients for the front baffle turned out to be 3-6% greater than for the lateral baffle at the same vertical distance in the combustion chamber, which is probably due to the smaller values of the incident radiation flux and, therefore, of the temperature of the ash deposits for the front baffle as well.

The longitudinal radiation fluxes through the horizontal transverse cross-sections of the combustion chamber have a considerable effect on the vertical distribution of temperatures and radiation fluxes (local heat transfer) in the combustion chamber. The considerable screening effect of the medium in the furnace (especially in the narrowing region) on the longitudinal radiative transfer in spectral intervals with high values of flame emissivity is evident from Table 3. It should be noted that the integral values of the longitudinal resulting radiation fluxes through the transverse cross-section reach magnitudes comparable to the magnitude of the resulting heat absorption by the furnace baffles.

An important indicator of the total heat transfer in the combustion chamber is the temperature of the gases at the furnace outlet. The results obtained show that with the calculation using the gray model, the decrease in temperature of the gases in the region of the outlet aperture is 58-89°C (76°C on the average over the cross section of the output aperture). The values of the radiation fluxes integrated over the spectrum for the gray model, on the other hand, are overestimated: incident up to 67 and resulting up to 30 kW/m^2.

NOTATION

σ_0, emission coefficient for an absolute blackbody, $W/m^2 \cdot K^4$; V and F, volume and surface area, respectively, of the volume and surface zone, m^3 and m^2; α, absorption coefficient, m^{-1}; f_{ij}^k, reduced resolution factor for radiation from zone i into zone j in spectral interval k; δ_{ij}, Kronecker's symbol; T, temperature, °K; ε, emissivity; μ_i^k, fraction of the energy emitted by an absolute blackbody at the temperature of zone i in spectral interval k, relative to the energy emitted over the entire spectral range examined; q^k, spectral radiation flux density, $W/cm^2 \cdot \mu m$; R_{av}, thermal resistance of ash deposits averaged over the furnace height, $m^2 \cdot °C/W$; H, height of the cooling chamber, m; h_i, vertical distance in the cooling chamber from the point at which it begins to the center of the computational region i, m; $F_{r,i}$, total surface area of the baffle surfaces in region i, m^2; $n = R'/R_{av}$ and $n'' = R''/R_{av}$, relative values of the thermal resistance of the ash deposits below and above the cooling chamber; λ, radiation wavelength, μm; m and n, number of volume and surface zones in the system; l, number of zones adjacent to zone j.

LITERATURE CITED

1. Yu. A. Zhuravlev, "Development of a zonal mathematical model of heat transfer in combustion chambers of boiler assemblies and investigation of its properties," Izv. Akad. Nauk SSSR, Energ. Transport, No. 6, 133-139 (1979).
2. Heat Calculations for Boilers (Standard Method) [in Russian], Énergiya, Moscow (1973).
3. A. G. Blokh, Thermal Radiation in Boiler Installations [in Russian], Énergiya, Leningrad (1967).
4. Yu. A. Popov and R. L. Shvartsblat, "Infrared absorption coefficient and index of refraction of carbon monoxide gas and water vapor," Teplofiz. Vys. Temp., 12, No. 6, 1188-1192 (1974).
5. C. B. Ludwig, W. Malkmus, T. E. Reardon, and A. L. Thomson, Handbook of Infrared Radiation from Combustion Gases, Washington, NASA (1973).
6. I. N. Konopel'ko, "Spectral emissivity of ash deposits in boiler combustion chambers," Energomashinostroenie, No. 11, 12-14 (1972).